Parameter estimation using unsteady downwash model from real flight data of Hansa-3 aircraft

R. Kumar **A. K. Ghosh**
rakpec@iitk.ac.in **akg@iitk.ac.in**
Aerospace Engineering Department at IIT-Kanpur
Kanpur, India

ABSTRACT

The paper presents the estimation of longitudinal aerodynamic parameters from simulated as well as real flight data using an unsteady downwash model. The task of parameter estimation was accomplished using the Maximum Likelihood (ML) method in the frequency domain for the Hansa-3 aircraft. The presented work pertains to the aircraft having a semi-sweptback wing configuration, however, the work reported earlier considered a rectangular wing configuration. A simple vortex system was used to model downwash effects in the longitudinal equations of motion. First, it was established that the indicial lift function had a minor or negligible influence on aircraft motion and on the estimated aerodynamic parameters using simulated data for the configuration of Hansa-3 aircraft. Next, two parameter extraction algorithms were used for parameter estimation using simulated data (with unsteadiness only in downwash) and real flight data (Hansa-3 aircraft). The first algorithm included unsteadiness only in downwash while the second neglected all the unsteady effects. It was observed from the results obtained that if unsteady effects were omitted from the parameter estimation algorithm, the extracted parameters included the effects of unsteady aerodynamics. Therefore, application of the extraction algorithm in the two modes provides a convenient means of separating steady-state and acceleration derivatives.

NOMENCLATURE

a_x, a_y, a_z	horizontal, lateral and vertical components of acceleration (m/s^2)
A	aspect ratio (-)
b	wing span (m)
$\overline{c}$	mean aerodynamic chord (m)
c_r	root chord (m)
c_t	tip chord (m)
C_L, C_m	lift and pitching moment coefficients (-)
$\tilde{\mathrm{D}}$	term used to model downwash in equations of motion (-)
f_1, f_2, f_3	factors associated with vortex system (-)
g	acceleration due to gravity (m/s^2)
F, G, H	coefficients used to model downwash (-)
$\tilde{\mathrm{I}}$	term used to model indicial lift in equations of motion (-)
I_y	moment of inertia about y-axis (kg-m^2)
J	cost function (-)
k	general index (-)
l	distance behind wing root quarter chord point (m)
l_t	horizontal tail moment arm (m)
m	aircraft mass (kg)
N	number of data points (-)
p, q, r	roll, pitch and yaw rates (rad/s)
R	measurement covariance matrix (-)
S	planform area (m^2)

Paper No. 3607. Manuscript received 2 July 2010, revised version received 24 March 2011, accepted 27 April 2011.

https://doi.org/10.1017/S0001924000006217 Published online by Cambridge University Press

t	time (s)
T	temperature (°C)
u	velocity (ms^{-1})
w	induced velocity (ms^{-1})
$\overline{x}$	distance downstream from a/c center of gravity to wing aerodynamic center (m)
y, z	constants based on geometry of the lifting surface (-)
Y	estimated value (-)
Z	measured value (-)
α	angle-of-attack (rad)
β	angle of slide slip (rad)
$\delta_a,\delta_e,\delta_r$	aileron, elevator and rudder deflection (rad)
Δ	bias (m)
$\Delta C_L(t)$	lift due to unit step change in α (-)
$\Delta\varepsilon(t)$	response in downwash due to unit step change in α (rad)
ε	downwash angle (rad)
$(\partial\varepsilon/\partial\alpha)_{l,ss}$	steady state downwash slope at a distance l (-)
Γ	circulation (m^3/s)
∞	infinity (-)
Λ	sweep angle (deg)
ω	frequency (rad/s)
φ, θ, ψ	angles of roll, pitch and yaw (rad)
ρ	density (kg/m^3)
Θ, ξ	vectors of unknown parameters (-)

Subscripts

f	fuselage
l	distance
ss	steady-state
t	horizontal tail
w	wing

Superscript

.	derivative with respect to time
~	variable in frequency domain

Abbreviations

ALGOPE	algorithm for parameter estimation
MAC	mean aerodynamic chord
RSP	real short period
SIMDAT	Asimulated data

Longitudinal stability and control derivatives

$$C_{L_\alpha}=\partial C_L/\partial\alpha,\qquad C_{L_q}=\partial C_L/\partial(qc/2u),\qquad C_{L_{\delta e}}=\partial C_L/\partial\delta e$$

$$C_{m_\alpha}=\partial C_m/\partial\alpha,\qquad C_{m_q}=\partial C_m/\partial(qc/2u),\qquad C_{m_{\delta e}}=\partial C_m/\partial\delta e$$

$$C_{m_{\dot\alpha}}=\partial C_m/\partial(\dot\alpha\bar{c}/2u)=-2(l/\bar{c}_w)^2\,(C_{L_\alpha})_{l,ss}(\partial\varepsilon/\partial\alpha)_{l,ss},$$

$$C'_{m_\alpha}=(C_{m_\alpha})_{ss}-(\rho S_w\bar{c}_w C_{m_{\dot\alpha}}C_{L_\alpha}/4m)$$

$$C'_{m_q}=(C_{m_q})_{ss}+C_{m_{\dot\alpha}}\qquad C_{m_{\delta e}}=(C_{m_{\delta e}})_{ss}-(\rho S_w\bar{c}_w C_{m_{\dot\alpha}}C_{L_{\delta e}})/4m$$

1.0 INTRODUCTION

Aerodynamic parameter estimation from real flight data is a routine task for many aerospace organisations. Parameter estimation[1-7] is the process of determining the best possible estimates of the parameters occurring in the model used to represent it. After a priori fix of the aerodynamic model, the next task of estimating parameters is, generally, attempted by three different but complimentary techniques: analytical methods, wind-tunnel methods and flight-test methods. At initial stages of aircraft design, analytical methods[7] provide the only convenient way of estimating the aircraft parameters. However, the accuracy of such theoretical estimates being relatively low, there is a need to verify these estimates with those obtained from wind tunnel and flight tests.

The problem with the conventional parameter estimation methods is the assumption of an exact aerodynamic model. The unsteady aerodynamics associated with the load build-up following a change in angle-of-attack is, generally, neglected during the modelling. This leads to the extraction of different numerical value of the same parameter under similar flight conditions. The paper aims at the application of an algorithm, based on downwash model, for parameter estimation which accounts for unsteady aerodynamics associated with load build-up to simulated and real flight data. The downwash model has been applied to the simulated and real flight data of Hansa-3 aircraft (Fig. 1) having a semi-sweptback wing configuration. The effect of indicial lift on the extracted parameters has also been studied using the simulated data for the configuration of Hansa-3 aircraft.

The longitudinal aerodynamic parameters of an aircraft are determined primarily by the lift forces on wing, horizontal tail and elevator. In case of unsteady motion, the force model consists of the circulatory flow associated with angle-of-attack variation and the curvature of the flow streamlines relative to the surface during pitching motion. The latter can be analysed by considering an equivalent system which replaces the airfoil and circular streamlines with a circular-arc airfoil in rectilinear flow. The effect of the force component due to instantaneous acceleration of non-circulatory potential flow is generally small and can be neglected. However, this effect could be important for ultra-light aircrafts.

An approximate indicial lift function[8] associated with circulation has been utilised for modelling the indicial effects while the use of a simple vortex system has been made to model the unsteady downwash effects into the rigid body longitudinal equations of motion for the configuration of Hansa-3 aircraft. Earlier, many attempts have been made to model the indicial and unsteady downwash effects in the longitudinal[9-14] as well as in the lateral[15-17] cases along with parameter estimation for rectangular wing configuration. But, the present work pertains to Hansa-3 aircraft having semi-sweptback wing configuration.

The presented study consists of unsteady downwash modelling, the development[9] of equations of motion in the frequency domain, the generation of simulated and real flight data, discussion of results and concluding remarks. Section 2·0 presents the unsteady downwash modelling for the configuration of Hansa-3 aircraft. The equations of motion in the frequency domain are given in Section 3·0 for the two cases (when indicial lift function is considered and when indicial lift function is neglected). Section 4·0 explains the procedure for the generation of simulated and real flight data along with estimation of coefficients used to model downwash effects in the longitudinal equations of motion. The estimation results have been presented and discussed in Section 5·0. This section consists of parameter estimation from simulated and real flight data using two parameter estimation algorithms. Section 6·0 highlights the concluding remarks and the scope for the future work.

2.0 UNSTEADY AERODYNAMIC MODELLING

The lift forces acting on the lifting surfaces (wing, horizontal tail and elevator) are responsible for the determination of longitudinal aerodynamic parameters of an aircraft. Unsteady aerodynamic forces on these surfaces are estimated through the use of indicial lift (lift response due to a unit step increment in effective angle-of-attack) at each surface. The indicial lift function ($\Delta C_L(t)$) can be expressed by an exponential equation of the following form[9].

$$\Delta C_L(t)=(C_{L\alpha})_{ss}\,(1-ye^{-zut/(c_r/2)}) \qquad \ldots(1)$$

https://doi.org/10.1017/S0001924000006217 Published online by Cambridge University Press

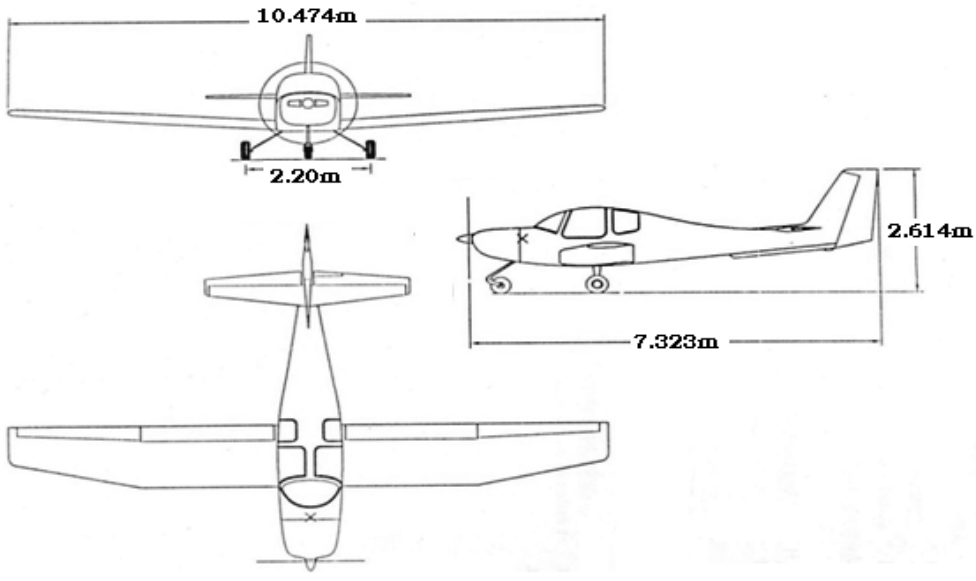


Figure 1. Three-view drawing of the Hansa-3 aircraft.

The term $(C_{L\alpha})_{ss}$ is steady state lift curve slope and the constants y and z are functions of geometry of the lifting surface[8].

The simplified vortex system (Fig. 2) has been used to calculate the downwash. The vortex system consists of a bound vortex along the wing quarter-chord line, a trailing vortex at each wing tip and a shed vortex connecting the downstream ends of the trailing vortices. The vortices were all in a plane parallel to the freestream direction. The vortex system stretched in the downstream direction at one-half of the freestream velocity. The vortex strength was same in all the portions of the system.

The downwash was calculated for the simple vortex system representation only in the plane of the vortex system, midway between the two trailing vortices. The downwash at a distance l downstream from the midpoint of the bound vortex can be determined by the use of the Biot-Savart law. Equation (2) presents the expression for the induced velocity[9] at a distance l.

$$w_l(t) = \Gamma/\pi c_r \,[f_1 + f_2(t) + f_3(t)] \qquad \ldots (2)$$

$$f_1 = \frac{c_r}{2l}\left\{\mathrm{Tan}\Lambda + \frac{\left[\frac{A(1+\lambda)}{4}\right]\mathrm{Sec}^2\Lambda - \frac{l}{c_r}\mathrm{Tan}\Lambda}{\sqrt{\left[\frac{A(1+\lambda)}{4\,\mathrm{Cos}\,\Lambda} - \frac{l}{c_r}\mathrm{Sin}\,\Lambda\right]^2 + \left(\frac{l}{c_r}\mathrm{Cos}\Lambda\right)^2}}\right\} \qquad \ldots (3(a))$$

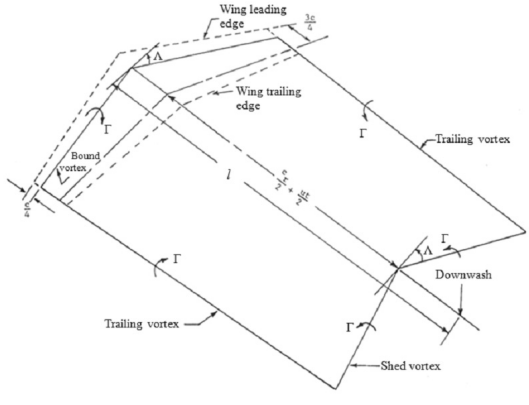


Figure 2. Vortex system used for computing downwash.

$$f_2(t) = \frac{2}{A(1+\lambda)}\left\{\frac{\frac{l}{c_r} - \left[\frac{A(1+\lambda)}{4}\right]\mathrm{Tan}\,\Lambda}{\sqrt{\left[\frac{l}{c_r} - \left[\frac{A(1+\lambda)}{4}\right]\mathrm{Tan}\,\Lambda\right]^2 + \left[\frac{A(1+\lambda)}{4}\right]^2}} - \frac{\frac{l}{c_r} - 1 - \frac{ut}{2c_r} - \left[\frac{A(1+\lambda)}{4}\right]\mathrm{Tan}\,\Lambda}{\sqrt{\left[\frac{l}{c_r} - 1 - \frac{ut}{2c_r} - \left[\frac{A(1+\lambda)}{4}\right]\mathrm{Tan}\,\Lambda\right]^2 + \left[\frac{A(1+\lambda)}{4}\right]^2}}\right\}$$

$\ldots (3(b))$

$$f_3(t) = \frac{1}{2\left(\frac{l}{c_r} - 1 - \frac{ut}{2c_r}\right)}\left\{\mathrm{Tan}\Lambda + \frac{\left[\frac{A(1+\lambda)}{4}\right]\mathrm{Sec}^2\Lambda - \left(\frac{l}{c_r} - 1 - \frac{ut}{2c_r}\right)\mathrm{Tan}\,\Lambda}{\sqrt{\left[\frac{A(1+\lambda)}{4\,\mathrm{Cos}\,\Lambda} - \left(\frac{l}{c_r} - 1 - \frac{ut}{2c_r}\right)\mathrm{Sin}\,\Lambda\right]^2 + \left[\left(\frac{l}{c_r} - 1 - \frac{ut}{2c_r}\right)\mathrm{Cos}\,\Lambda\right]^2}}\right\}$$

$\ldots (3(c))$

In Equation (2), f_1 is associated with the quarter-chord line bound vortex, $f_2(t)$ is associated with the two wing-tip vortices and $f_3(t)$ is associated with the shed vortex. The quantities A (8·8), cr (1·3), Λ (6 deg) and λ (0·8) are aspect ratio, root chord, sweep angle and taper ratio of the wing, respectively. Figure 3 presents the variation of factors associated with the simple vortex system (f_1, f_2 and f_3) with time for the Hansa-3 aircraft.

Use of the Kutta-Joukowski equation in the Equation (2) leads to the following expression[9].

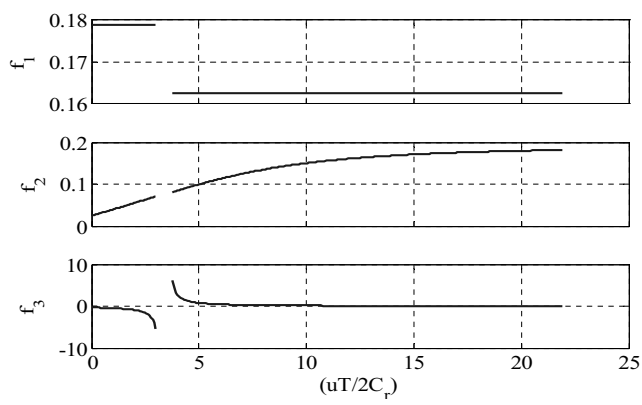


Figure 3. Variation of f_1, f_2, f_3 with time.

https://doi.org/10.1017/S0001924000006217 Published online by Cambridge University Press

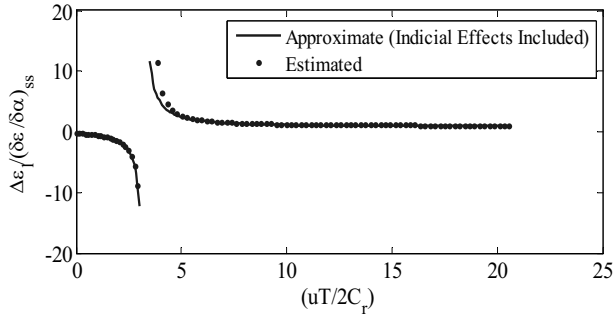


Figure 4. Approximate and estimated response of downwash (indicial lift included).

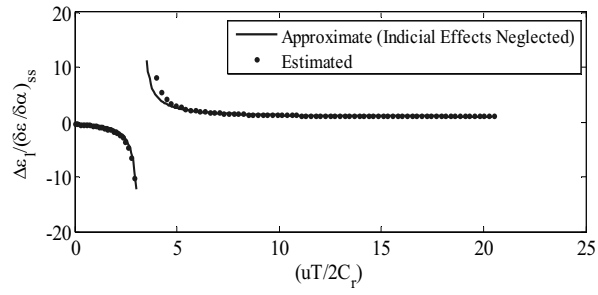


Figure 5. Approximate and estimated response of downwash (indicial lift neglected).

$$w_l(t) = U(1+\lambda)/4\pi\, C_L(t)[f_1 + f_2(t) + f_3(t)] \quad \ldots (4)$$

The following equation defines the downwash angle.

$$\varepsilon_l(t) = w_l(t)/u \quad \ldots (5)$$

Equation (6) presents the expression for the downwash following a unit step increase in the angle-of-attack[9].

$$\Delta\varepsilon_l(t) = (1+\lambda)/4\pi\, \Delta C_L(t)[f_1 + f_2(t) + f_3(t)] \quad \ldots (6)$$

Substitution of Equation (1) into Equation (6) results in Equation (7)

$$\Delta\varepsilon_l(t) = (1+\lambda)/4\pi (C_L\alpha)_{ss}(1 - ye^{-zut/(cr/2)})[f_1 + f_2(t) + f_3(t)] \quad \ldots (7)$$

The vortex system being used was a simple model for a complex physical system. The accuracy of Equation (7) can be established by assuring the correctness at known steady-state conditions. The expression for downwash in terms of steady-state value is given by[9]:

$$\Delta\varepsilon_l(t) = (\partial\varepsilon/\partial\alpha)_{l,ss}(1 - ye^{-zut/cr2})\,[(f_1 + f_2(t) + f_3(t)) / (f_1 + f_2(\infty) + f_3(\infty)] \quad \ldots (8)$$

The quantities $f_2(\infty)$ and $f_3(\infty)$ evaluated by letting $t \to \infty$ in Eqs (2(b) and 2(c)) result in the following expressions;

$$f_2(\infty) = \frac{2}{A(1+\lambda)}\left\{\frac{\frac{l}{c_r} - \left[\frac{A(1+\lambda)}{4}\right]\mathrm{Tan}\,\Lambda}{\sqrt{\left[\frac{l}{c_r} - \left[\frac{A(1+\lambda)}{4}\right]\mathrm{Tan}\,\Lambda\right]^2 + \left[\frac{A(1+\lambda)}{4}\right]^2}} + 1\right\} \quad f_3(\infty) = 0$$

The complicated form of Equation (8) can be approximated very closely by the following Equation (9).

$$\Delta\varepsilon_l(t) = \left(\frac{\partial\varepsilon}{\partial\alpha}\right)_{l,ss}\left[1 - \frac{F}{\left(\frac{l}{c_r}-1\right)-\frac{ut}{2c_r}} - Ge^{-H\frac{ut}{c_r/2}}\right] \quad \ldots (9)$$

Equation (9) is in a convenient form for the use in frequency response calculation, because Fast Fourier transforms are available for the terms involved. The values of *F, G* and *H* are functions of the wing geometry and the length *l* and can be determined by curve fitting Equation (9) to the results calculated from Equation (8).

The downwash for an arbitrary angle-of-attack can be obtained by the use of equation (9) in Duhamel's integral and is given by[9]:

$$\varepsilon_l(t) = \left(\frac{\partial\varepsilon}{\partial\alpha}\right)_{l,ss}\int_0^t\left[1 - \frac{F_w'}{\left(\frac{l}{c_{r_w}}-1\right)-\frac{u(t-\tau)}{2c_{r_w}}} - G_w'e^{-H_w'\frac{u(t-\tau)}{c_{r_w}/2}}\right]\dot{\alpha}(t)d\tau \quad \ldots (10)$$

The quantities c_{r_w}, $\dot{\alpha}$ and $(\partial\varepsilon/\partial\alpha)_{l,ss}$ are the wing root chord, rate of change of angle-of-attack and change in steady state value of downwash angle with change in angle-of-attack, respectively.

The unsteady downwash ($\Delta\varepsilon_l(t)$) following a unit step increase in angle-of-attack is given by Equation (8). The expression for ($\Delta\varepsilon_l(t)$) was used in Duhamel's integral [Equation (10)] to calculate downwash ($\varepsilon_l(t)$) at location *l*. It was found that the expression given in Equation (8) was not in a suitable form to be used in the estimation algorithm for the purpose of parameter estimation. It has been proved[9] that the downwash Equation (8) could be approximated very closely by Equation (9). Therefore, the model represented by Equation (9) was used to incorporate indicial plus unsteadiness in downwash and unsteadiness only in downwash in the equations of motion given by Equation (16) and Equation (19), respectively in terms of coefficients *F*, *G* and *H*.

Table 1
Characteristics of Hansa-3 aircraft

Item (symbol)	Value (units)
Wing	
planform area (S_w)	12·47 (m^2)
aspect ratio (A_w)	8·8
MAC ($\bar{c}_w$)	1·21 (m)
root chord (c_{r_w})	1·3 (m)
tip chord (c_{t_w})	0·8 (m)
span (b)	10·47 (m)
taper ratio (λ_w)	0·8
sweep angle (Λ)	6 (deg)
Horizontal tail	
planform area (St)	2·04 (m^2)
aspect ratio (A_t)	6·35
taper ratio (λ_t)	0·454
root chord (c_{r_t})	0·78 (m)
tip chord (c_{t_t})	0·354 (m)
MAC ($\bar{c}_t$)	0·59 (m)
Aircraft	
Mass (m)	750kg
velocity (u)	47·5ms^{-1}
moment of inertia (I_y)	925kg-m^2
moment arm (l_t)	3·624m
distance behind wing root ($c_{1/4}$) point (l)	3·2m
density (ρ)	0·96(kg/m^3)

https://doi.org/10.1017/S0001924000006217 Published online by Cambridge University Press

Aerodynamic characteristics		
$(C_{L_\alpha})_{w,ss}$		4·6
$(C_{L_\alpha})_{t,ss}$		0·48
$(C_{m_\alpha})_{f,ss}$		0·3
$(C_{L_\alpha})_{t,ss}$	$(\partial\varepsilon/\partial\alpha)_{t,ss}$	0·22

Table 1 presents the geometric, mass, inertia and aerodynamic characteristics of the Hansa-3 aircraft used for the presented analysis. The data generated by the use of Equation (8) for the configuration of the Hansa-3 aircraft was considered as measured data. The data generated by Equation (8) as a function of time included indicial plus unsteady downwash effects when the values of constants y and z used were non-zero and included unsteadiness only in downwash when the values of y and z used were equal to zero. The constants y and z used to estimate the coefficients F, G and H were calculated using the formulations given in Ref. 8. The calculated value of constants y and z were 0·392 and 0·341, respectively when the indicial effects were considered while retaining the unsteadiness in downwash for both the cases.

Both the data were used to estimate F, G and H using the model represented by Equation (9). The ML method was used to minimise the error between measured [Equation (8)] and estimated [Equation (9)] output to obtain the coefficients. Later, these estimated coefficients were used to model the indicial and unsteady downwash effects in the simulated flight data and estimation algorithms.

A well matched comparison between approximate [Equation (8)] downwash response and the downwash response generated by using the estimated coefficients [Equation (9)] has been presented as a function of time in Fig. 4 when the indicial lift effects were considered and in Fig. 5 when the indicial lift effects were omitted.

The estimated values of coefficients F, G and H using Equation (9) and the ML method are presented in Table 2 for both the cases [considering (y = 0·392, z = 0·341) and neglecting ($y = z = 0$) the indicial effects while retaining unsteadiness in downwash].

Table 2
Estimated Values of *F*, *G* and *H*

Indicial effects included		Indicial effects neglected	
Coefficients	**Value**	**Coefficients**	**Value**
F	1·6	F	1·3
G	0·56	G	0·3
H	0·031	H	0·031

2.1 Lift for an arbitrary variation of the angle-of-attack

The lift associated with an arbitrary variation in angle-of-attack of a wing can be obtained by using Equation (1).

$$C_{L_w}(t) = \left(C_{L_\alpha}\right)_{w,ss} \int_0^t \left(1 - y_w e^{-\frac{z_w u(t-\tau)}{c_{r_w}/2}}\right)\left[\dot{\alpha}(\tau) + \left(\bar{x} + \frac{\bar{c}_w}{2}\right)\frac{\dot{q}(\tau)}{u}\right] d\tau$$

where $$(\alpha_E)_w = \alpha + \frac{q}{u}\left(\bar{x} + \frac{\bar{c}_w}{2}\right) \quad \ldots (11)$$

The quantities α, $(\alpha_E)_w$, q, u, $\bar{c}_w$ and $\bar{x}$ are the angle-of-attack, the effective angle-of-attack of the wing, pitch rate, forward speed, mean aerodynamic chord of the wing and the distance downstream from aircraft center of gravity to the wing aerodynamic center respectively.

The lift on the horizontal tail behind the wing is given by[9]:

$$C_{L_t}(t) = \left(C_{L_\alpha}\right)_{t,ss} \int_0^t \left(1 - y_t e^{-\frac{z_t u(t-\tau)}{c_{r_t}/2}}\right)\left[\dot{\alpha}(\tau) + \left(l_t + \frac{\bar{c}_t}{2}\right)\frac{\dot{q}(\tau)}{u} - \dot{\varepsilon}_l(\tau)\right] d\tau$$

where $$(\alpha_E)_t = \alpha + \frac{q}{u}\left(l_t + \frac{\bar{c}_t}{2}\right) - (\varepsilon_l)_t \quad \ldots (12)$$

The quantities $(\alpha_E)_t$, $\bar{c}_t$, l_t and ε_l are the effective angle attack of the horizontal tail, mean aerodynamic chord of the horizontal tail, the moment arm and downwash due to the wing at a distance l (distance behind wing root quarter chord point), respectively.

Similarly, the lift for an arbitrary variation in elevator control deflection is given by[9]:

$$C_{L_e}(t) = \int_0^t \Delta C_{L_e}(t-\tau)\,\dot{\delta}_e(\tau) d\tau \quad \ldots (13)$$

The quantities $\dot{\delta}_e$, ΔC_{L_e}, τ and t are the time rate of elevator deflection, the elevator lift due to unit step change in α, time constant and time, respectively.

3.0 EQUATIONS OF MOTION

Assuming the initial pitch attitude and its variations to be small, the rigid-body longitudinal equations of motion are given by:

$$\dot{\alpha}(t) = q(t) - \rho u S_w/2m\, C_L(t) \quad \ldots (14(a))$$

$$\dot{q}(t) = \rho u^2 S_w \bar{c}_w/2I_y\, C_m(t) \quad \ldots (14(b))$$

The unsteady aerodynamic effects modeled in the terms $C_L(t)$ and $C_m(t)$ is expressed as:

$$C_L(t) = C_{Lw}(t) + C_{Lt}(t) + C_{Le}(t) \quad \ldots (15(a))$$

$$C_m(t) = -\frac{l_t}{\bar{c}_w}\left[C_{L_t}(t) + C_{L_e}(t)\right] + \left(C_{m_\alpha}\right)_f \alpha - \frac{\bar{x}}{\bar{c}_w} C_{L_w}(t) \quad \ldots (15(b))$$

The resulting pair of integro-differential equations, after substitution in Equation (15), involves the convolution integrals, the solution of which becomes very cumbersome and time consuming. Therefore, the equations of motion were transformed in the frequency domain to simplify them and make them more suitable for use in parameter estimation.

3.1 When indicial lift is considered

The matrix form of the equations of motion in the frequency domain, while considering the indicial lift, can be expressed as[9]:

$$\begin{bmatrix} \frac{\tilde{\alpha}}{\tilde{\delta}_e} \\ \frac{\tilde{q}}{\tilde{\delta}_e} \end{bmatrix} = \begin{bmatrix} A'_{11} & A'_{12} \\ A'_{21} & A'_{22} \end{bmatrix}^{-1} \begin{bmatrix} -\frac{\rho u S_w}{2m}\tilde{C}_{L_e} \\ -\frac{\rho u^2 S_w \bar{c}_w}{2I_y}\tilde{C}_{L_e} \end{bmatrix} \quad \ldots (16)$$

where

$$A'_{11} = i\omega + \frac{\rho u S_w}{2m}\left(\tilde{C}_{L_w} + \tilde{C}_{L_{t_1}}\right) \quad \ldots (17(a))$$

$$A'_{12} = -1 + \frac{\rho S_w}{2m}\left[\left(\bar{x} + \frac{\bar{c}_w}{2}\right)\tilde{C}_{L_w} + \left(l_t + \frac{\bar{c}_t}{2}\right)\tilde{C}_{L_{t_2}}\right] \quad \ldots (17(b))$$

$$A'_{21} = \frac{\rho u^2 S_w \bar{c}_w}{2I_y}\left[\left(\frac{\bar{x}}{\bar{c}_w}\tilde{C}_{L_w} + \frac{l_t}{\bar{c}_w}\tilde{C}_{L_{t_1}}\right) - \left(\tilde{C}_{m_\alpha}\right)_f\right] \quad \ldots (17(c))$$

$$A'_{22} = i\omega + \frac{\rho u S_w}{2I_y}\left[\left(\bar{x} + \frac{\bar{c}_w}{2}\right)\bar{x}\tilde{C}_{L_w} + \left(l_t + \frac{\bar{c}_t}{2}\right) l_t \tilde{C}_{L_{t_2}}\right] \quad \ldots (17(d))$$

https://doi.org/10.1017/S0001924000006217 Published online by Cambridge University Press

$$\tilde{C}_{L_w} = \left(C_{L_\alpha}\right)_{w,ss}\left(1 - \frac{i\omega y_w}{i\omega + \frac{z_w u}{c_{r_w}/2}}\right) \quad \ldots (18(a))$$

$$\tilde{C}_{L_{t_1}} = \left(C_{L_\alpha}\right)_{t,ss}\left(1 - \frac{i\omega y_t}{i\omega + \frac{z_t u}{c_{r_t}/2}}\right)\left\{\left[1 - \left(\frac{\partial\varepsilon}{\partial\alpha}\right)_{l,ss}\right] + \left(\frac{\partial\varepsilon}{\partial\alpha}\right)_{l,ss}\tilde{D}\right\} \quad \ldots (18(b))$$

$$\tilde{C}_{L_{t_2}} = \left(C_{L_\alpha}\right)_{t,ss}\left(1 - \frac{i\omega y_t}{i\omega + \frac{z_t u}{c_{r_t}/2}}\right) \quad \ldots (18(c))$$

$$\tilde{C}_{L_e} = \left(C_{L_{\delta_e}}\right)_{ss}\left(1 - \frac{i\omega y_e}{i\omega + \frac{z_e u}{c_{r_e}/2}}\right) \quad \ldots (18(d))$$

$$\tilde{D} = \left[\frac{2i\omega F'_w}{u/c_{r_w}} e^{-\left(2\frac{l-c_{r_w}}{u}\right)i\omega}\right]\left[E_i\left(2\frac{l-c_{r_w}}{u}\right)i\omega\right] + \frac{i\omega G'_w}{i\omega + \frac{H'_w u}{c_{r_w}/2}} \quad \ldots (18(e))$$

3.2 When indicial lift is omitted

Equation (16) does not contain the parameters explicitly, thereby, making it unsuitable for parameter estimation. Therefore, the terms involved in Equation (16) are modified in such a manner that it represents the desired aerodynamic model. Equation (19) presents the resulting matrix form[9] of the equations of motion in the frequency domain, while neglecting the indicial lift.

$$\begin{bmatrix}\frac{\tilde{\alpha}}{\tilde{\delta}_e}\\ \frac{\tilde{q}}{\tilde{\delta}_e}\end{bmatrix} = \begin{bmatrix}A_{11} & A_{12}\\ A_{21} & A_{22}\end{bmatrix}^{-1}\begin{bmatrix}-\frac{\rho u S_w}{2m}\left(C_{L_{\delta_e}}\right)_{ss}\\ -\frac{\rho u^2 S_w \bar{c}_w}{2I_y}\left(C_{m_{\delta_e}}\right)_{ss}\end{bmatrix} \quad \ldots (19)$$

where

$$A_{11} = i\omega + \frac{\rho u S_w}{2m}\left[\left(C_{L_\alpha}\right)_{ss} + \left(C_{L_\alpha}\right)_{t,ss}\left(\frac{\partial\varepsilon}{\partial\alpha}\right)_{l,ss}\tilde{D}\right] \quad \ldots (20(a))$$

$$A_{12} = -1 + \frac{\rho S_w \bar{c}_w}{4m}\left(C_{L_q}\right)_{ss} \quad \ldots (20(b))$$

$$A_{21} = -\frac{\rho u^2 S_w \bar{c}_w}{2I_y}\left[\left(C_{m_\alpha}\right)_{ss} - \frac{l_t}{\bar{c}_w}\left(C_{L_\alpha}\right)_{t,ss}\left(\frac{\partial\varepsilon}{\partial\alpha}\right)_{l,ss}\tilde{D}\right] \quad \ldots (20(c))$$

$$A_{22} = i\omega - \frac{\rho u S_w \bar{c}_w^2}{4I_y}\left(C_{m_q}\right)_{ss} \quad \ldots (20(d))$$

$$\tilde{D} = \left[\frac{2i\omega F_w}{u/c_{r_w}} e^{-\left(2\frac{l-c_{r_w}}{u}\right)i\omega}\right]\left[E_i\left(2\frac{l-c_{r_w}}{u}\right)i\omega\right] + \frac{i\omega G_w}{i\omega + \frac{H_w u}{c_{r_w}/2}} \quad \ldots (20(e))$$

The vertical acceleration used in the process of data simulation and parameter estimation can be obtained by using the following equation.

$$\tilde{a}_z = u/g\,(i\omega\tilde{\alpha} - \tilde{q}) \quad \ldots (21)$$

4.0 GENERATION OF FLIGHT DATA: HANSA-3 AIRCRAFT

The simulated data were generated for the Hansa-3 model while the real flight data were generated by conducting the actual flight testing (Hansa-3 aircraft) at the flight laboratory of the Indian Institute of Technology, Kanpur. The aerodynamic models were applied to simulated and real flight data for the estimation of aerodynamic parameters.

4.1 Simulated flight data

The two types of flight data (angle-of-attack (α), pitch rate (q) and vertical acceleration (a_z)) were simulated in the frequency domain for the Hansa-3 aircraft for unit step elevator deflection (δ_e). First flight data simulated for unit step elevator deflection in the frequency domain included indicial lift function ($\tilde{I} \neq 0$) and unsteadiness in downwash ($\tilde{D} \neq 0$) while the second simulated flight data excluded the indicial lift function ($\tilde{I} = 0$) but retained unsteadiness in downwash ($\tilde{D} \neq 0$). The first ($\tilde{I} \neq \tilde{D} \neq 0$) and the second ($\tilde{I} = 0$, $\tilde{D} \neq 0$) simulated data have been referred to as SIMDATA1 and SIMDATA2, respectively in the rest of the presented work. The matrix forms of Equation (16) and Equation

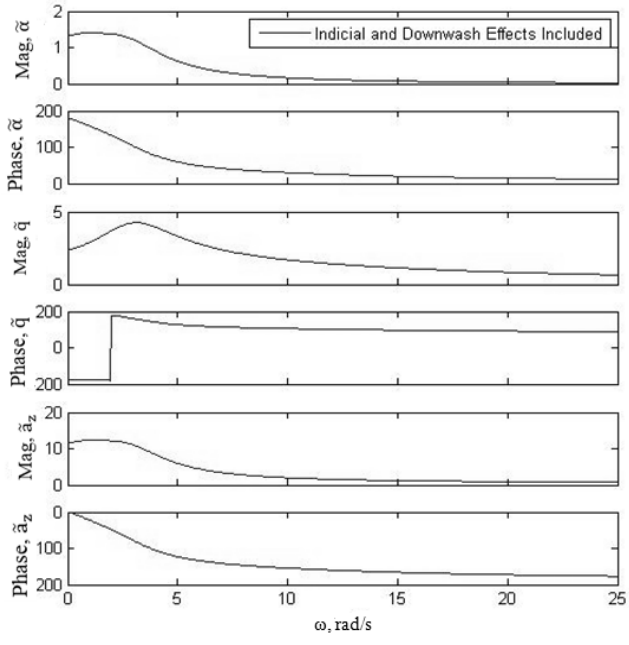


Figure 6. Simulated data ($\tilde{I} \neq \tilde{D} \neq 0$); SIMDATA1.

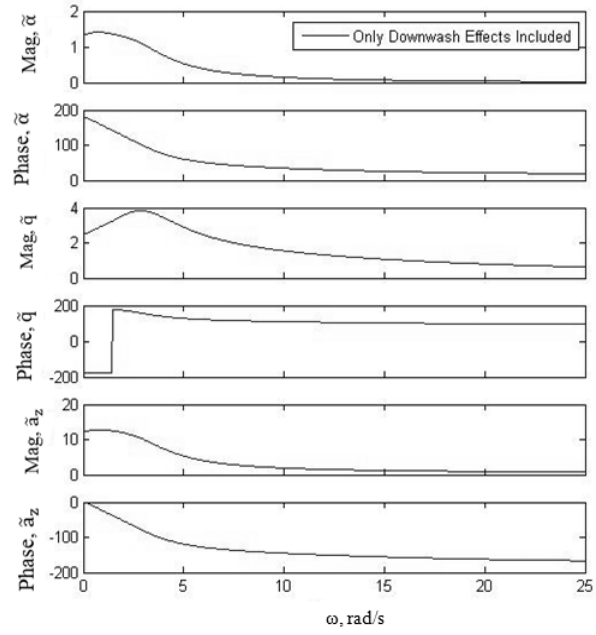


Figure 7. Simulated data ($\tilde{I} = 0$, $\tilde{D} \neq 0$); SIMDATA2.

https://doi.org/10.1017/S0001924000006217 Published online by Cambridge University Press

(19) along with Equation (21) were used to generate the simulated data sets SIMDATA1 and SIMDATA2, respectively. The geometric, mass, inertia and aerodynamic characteristics used to simulate SIMDATA1 and SIMDATA2 are shown in Table 1.

Next, the use of geometric, mass, inertia and aerodynamic characteristics (Table 1) of the Hansa-3 aircraft and the estimated coefficients (Table 2) allowed us to generate simulated data sets SIMDATA1 and SIMDATA2· The steady state values of aerodynamic derivatives used to simulate the flight data are given in Table 4. The matrix forms of Equation (16) and Equation (19), along with Equation (21), were used to simulate SIMDATA1 and SIMDATA2, respectively.

Figure 6 presents SIMDATA1 showing the variation of magnitude and phase of angle-of-attack (α), pitch rate (q) and vertical acceleration (a_z) with frequency for unit step elevator deflection (δ_e) while considering indicial and unsteady downwash effects. Figure 7 presents the SIMDATA2 showing the variation of magnitude and phase of α, q and a_z with frequency for unit step elevator deflection (δ_e) while neglecting the indicial lift effects for the configuration of Hansa-3 aircraft.

The data sets SIMDATA1 and SIMDATA2 have also been used to investigate the effect of the indicial lift function on the estimated parameters and aircraft motion. This showed negligible effects of indicial lift on parameter estimates and SIMDATA2 was therefore used for all later work involving parameter estimation.

4.2 Real flight data

A flight test program was carried out at the Indian Institute of Technology, Kanpur to obtain the real flight data of the Hansa-3 aircraft. An onboard measurement system installed on the test aircraft provided measurements using dedicated sensors for a large number of signals such as aircraft motion variables, atmospheric conditions, control surface deflections etc. The measurements made in flight were recorded on board at a sampling rate of 50Hz using a suitable interface with a standard Laptop computer and Labview software.

The flight data consisted of raw data for the measured variables u, α, β, p, q, r, a_x, a_y, a_z, φ, θ, ψ, H, δ_a, δ_e and δ_r and the location of the sensors used for the measurements. The measurements of u, α and β were obtained with flight log mounted on a boom fixed to the tip of the wing. The accelerations (a_x, a_y, a_z) along the three body axes were measured using an accelerometer located near the centre of gravity of the aircraft. The angular rates p, q and r were obtained from the measurements available from the inertial platform. The angular rates $\dot{p}$, $\dot{q}$ and $\dot{r}$ were obtained by the numerical differentiations of the corresponding angular rates. The control surface deflections (δ_a, δ_e and δ_r) were measured using potentiometers. The temperature T was recorded using the standard cockpit outside air temperature (OAT) gauze. The calibration coefficients obtained during the calibration of sensors, before conducting the flight tests, were used to process the raw real flight data.

After establishing a typical cruise at desired altitude, elevator deflection inputs were used to excite the longitudinal dynamics of the aeroplane. Five real flight data sets (RSP1, RSP2, RSP3, RSP4 and EP1 defined as real short period mode excited by using 3-2-1-1 (first four sets) and pulse elevator control input) were generated which consisted of time histories of various measured state and motion variables.

Data compatibility checks, also referred to as Flight path reconstruction (FPR), were carried out to ensure that the measurements used for subsequent aerodynamic model identification were consistent and error free[7]. The scale factors and zero shifts present in the measured flight variables were estimated using observation equations and the ML algorithm. The methodology and formulations described in Ref. 7 were used to carry out the data compatibility check on real flight data.

The following set of unknown parameters was considered adequate for reconstructing the longitudinal dynamics of the Hansa-3 aircraft for a data compatibility check.

$$\Theta = [\Delta a_x \quad \Delta a_y \quad \Delta a_z \quad \Delta p \quad \Delta q \quad \Delta r \quad K_\alpha \quad \Delta\alpha]^T \qquad \ldots (22)$$

Table 3 presents the compatibility factors estimated after carrying out a data compatibility check on real flight data using the ML method. The Cramer-Rao bounds used to assess the level of accuracy of the estimates is a by-product of the ML method. Ideally, the real flight data is assumed to be of good quality if the estimated values of biases and scale factors are found to be negligible and close to unity, respectively.

It can be observed (Table 3) that the estimated value of biases such as Δa_x, Δa_y, Δa_z, Δp, Δq, Δr $\Delta\alpha$ and K_α are negligible and the estimated value of scale factor, Kα, is close to unity for all the five real flight data sets (RSP1, RSP2, RSP3, RSP4 and EP1) as desired. These estimated compatibility factors were incorporated in the real flight data to make the data compatible for the purpose of parameter estimation. The low/negligible values of the Cramer-Rao bounds establish the accuracy of estimation of the compatibility factors.

Table 3
Data compatibility check for longitudinal real flight data of Hansa-3 aircraft

		Real flight data sets				
Parameters	**Units**	**RSP1**	**RSP2**	**RSP3**	**RSP4**	**EP1**
Δa_x	m/s^2	3·95e–1	8·07e–2	3·46e–1	3·66e–1	3·20e–1
		(6·22e–2)	(8·07e–2)	(5·17e–2)	(5·21e–3)	(2·17e–3)
Δa_y	m/s^2	2·24e–1	–2·65e–2	3·73e–1	–2·16e–1	7·22e–3
		(1·27e–3)	(1·62e–3)	(9·37e–4)	(1·93e–3)	(1·56e–3)
Δa_z	m/s^2	–3·20e–2	1·10e–2	–1·77e–3	–1·52e–2	–1·05e–2
		(2·05e–3)	(1·68e–3)	(1·36e–3)	(2·45e–3)	(1·13e–3)
Δp	rad/s	2·55e–3	–7·56e–4	–1·40e–4	1·91e–3	–1·92e–5
		(7·05e–6)	(1·68e–5)	(5·71e–6)	(1·13e–5)	(1·75e–5)
Δq	rad/s	1·83e–3	–9·05e–4	1·68e–5	–7·37e–4	1·04e–3
		(1·83e–5)	(1·05e–5)	(3·50e–6)	(1·89e–5)	(1·46e–5)
Δr	rad/s	8·21e–3	3·04e–3	1·13e–3	–5·97e–3	6·65e–4
		(1·84e–5)	(2·57e–5)	(5·83e–6)	(2·40e–5)	(1·95e–5)
K_α	–	1·09e+0	1·02e+0	9·91e–1	9·90e–1	1·01e+0
		(9·79e–3)	(8·09e–3)	(8·30e–3)	(1·17e–2)	(1·55e–2)
Δα	rad	–2·09e–3	–4·77e–3	3·72e–3	2·32e–3	–1·12e–3
		(6·20e–4)	(6·34e–4)	(1·03e–3)	(7·15e–4)	(9·28e–4)

( ) Cramer-Rao Bound

Figures 8-11 present the compatible data showing the time variation of the angle-of-attack (α), pitch rate (q) and vertical acceleration (a_z) generated by using 3-2-1-1 elevator deflection (δ_e) for the first four data sets (RSP1, RSP2, RSP3 and RSP4). The variation of the state variables (α, q and a_z) presented for the fifth data set (EP1) in Fig. 12 used the pulse elevator control input. The units of the variables α, q, a_z and δ_e shown in the Figures 8-11 are degree, degree/s, m/s^2 and degree respectively. The state variables for all the five real flight data sets were converted in the frequency domain using the Fast Fourier transforms for the given elevator control input. Later, the data converted in the frequency domain was used for the intended task of parameter estimation using two parameter estimation algorithms. The first algorithm included unsteadiness only in downwash ($\tilde{D} \neq 0$) whereas the second neglected all the unsteady effects ($\tilde{D} = 0$). Both the estimation algorithms neglected the indicial lift effects. The first ($\tilde{D} \neq 0$) and the second ($\tilde{D} \neq 0$) algorithms used for parameter estimation are referred to as ALGOPE1 and ALGOPE2, respectively for the rest of the presented analysis.

https://doi.org/10.1017/S0001924000006217 Published online by Cambridge University Press

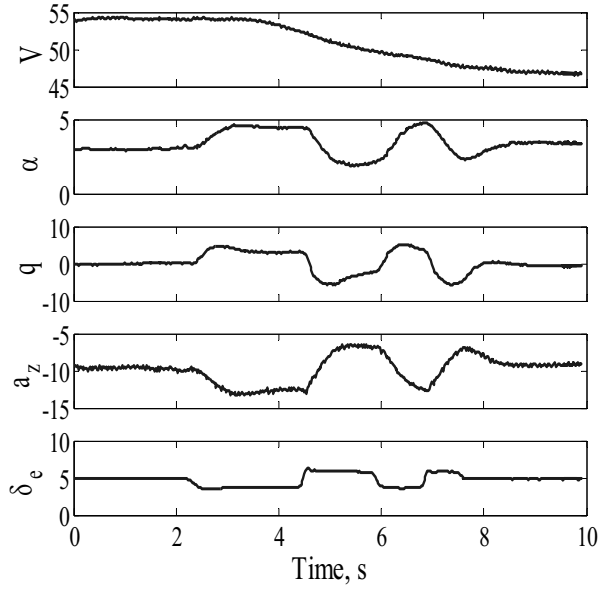


Figure 8. Real flight data of Hansa-3 aircraft; RSP1.

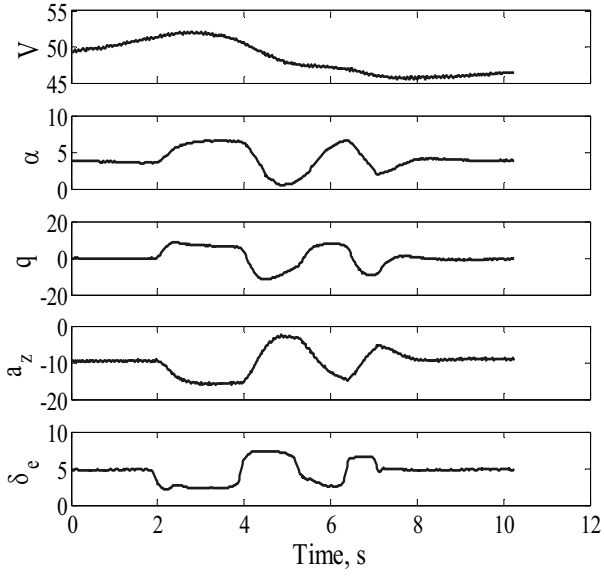


Figure 9. Real flight data of Hansa-3 aircraft; RSP2.

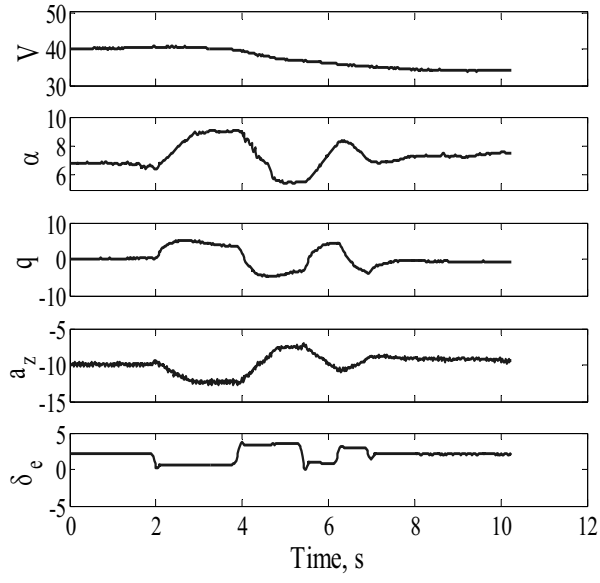


Figure 10. Real flight data of Hansa-3 aircraft; RSP3.

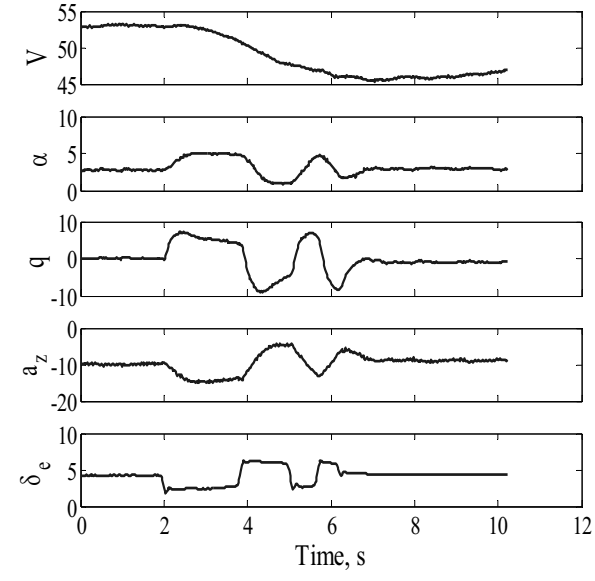


Figure 11. Real flight data of Hansa-3 aircraft; RSP4.

5.0 RESULTS AND DISCUSSION

An unsteady downwash model using simplified vortex system was applied to the simulated and the real flight data of the Hansa-3 aircraft for parameter estimation. Before the application of the unsteady downwash model to the simulated and real flight data of the Hansa-3 aircraft for parameter estimation, it was established that the indicial lift function has a very little or negligible effect on aircraft motion and estimated parameters. Therefore, the indicial component was omitted from the original model (Equation (16)), along with certain modifications, to make the downwash model suitable for parameter estimation (Equation (19)).

5.1 Effect of indicial lift function on extracted parameters

The effect of neglecting the indicial response has been examined by determining (1) whether the indicial lift has any effect on the aircraft frequency-response characteristics and (2) whether the indicial lift function influences the numerical value of the estimated parameters. SIMDATA1 and SIMDATA2 (generated in the foregoing section) in the frequency domain for the configuration of the Hansa-3 aircraft was now used for the parameter estimation using ALGOPE1 [Equation (19)] and the ML method. ALGOPE1 was used to estimate the parameter vector (ξ) given by Equation (23)

$$\xi = [C_{L_\alpha}\ C_{L_q}\ C_{L_{\delta e}}\ C_{m_\alpha}\ C_{m_q}\ C_{m_{\delta e}}]^T \quad \ldots (23)$$

The cost function given by Equation (24) was minimised using the ML method to estimate ξ.

$$J(\xi, R) = \tfrac{1}{2} \sum_{K=1}^{N} [Z(k) - Y(k)]^T R^{-1} [Z(k) - Y(k)] \quad \ldots (24)$$

$$R = \tfrac{1}{N} \sum_{K=1}^{N} [Z(k) - Y(k)] [Z(k) - Y(k)]^T \quad \ldots (25)$$

https://doi.org/10.1017/S0001924000006217 Published online by Cambridge University Press

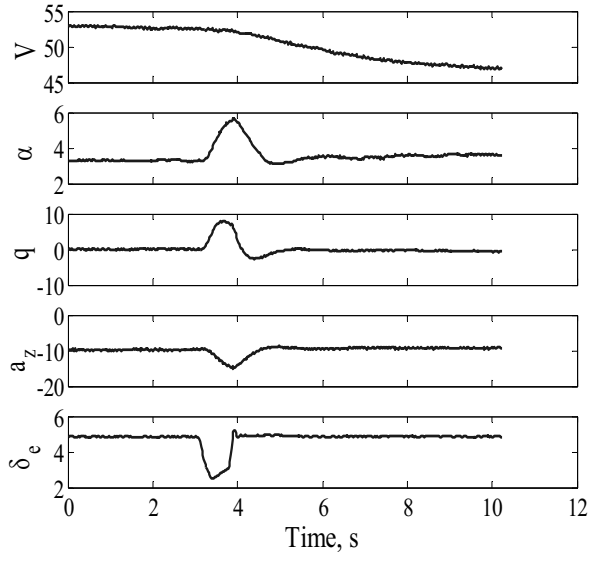


Figure 12. Real flight data of Hansa-3 aircraft; E_P1.

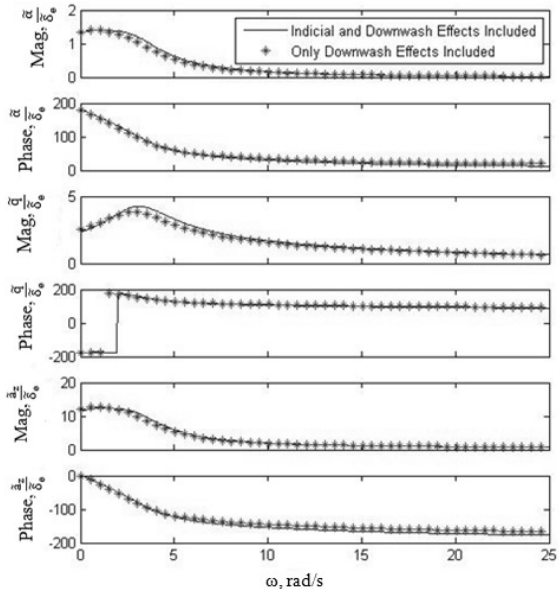


Figure 13. Comparison of magnitude and phase response ($\tilde{\alpha}/\tilde{\delta}_e$), ($\tilde{q}/\tilde{\delta}_e$) and ($\tilde{a}_z/\tilde{\delta}_e$).

The terms R, $Z(k)$ and $Y(k)$ are defined as measurement covariance matrix, measured and estimated output at k^{th} instant respectively. N and k are number of data points and general index for data points respectively.

Table 4 presents the values of the parameters estimated from simulated flight data SIMDATA1 using estimation algorithm ALGOPE1. It can be observed (Table 4) that the parameters estimated from SIMDATA1 using ALGOPE1 are in close agreement with the true values except the parameter C_{Lq}. It has been found that the parameter C_{Lq} has only a minor or negligible effect on the aeroplane motion.

Table 4
Parameter estimation using SIMDATA1 and ALGOPE1

Parameters [True value]	Estimated Value
$C_{L\alpha}$ [5·0]	5·0 (0·0)
C_{Lq} [7·0]	0·88 (0·0)
$C_{L\delta e}$ [0·3]	0·29 (0·0)
$C_{m\alpha}$ [–0·4]	–0·41 (0·0)
C_{mq} [–8·0]	–7·52 (0·0)
$C_{m\delta e}$ [–0·8]	–0·83 (0·0)

( ) Cramer-Rao bounds

Figure 13 compares the frequency-response characteristics of the angle-of-attack ($\tilde{\alpha}/\tilde{\delta}_e$), pitch rate ($\tilde{q}/\tilde{\delta}_e$) and vertical acceleration ($\tilde{a}_z/\tilde{\delta}_e$) for a unit step elevator control input in terms of magnitude and phase generated by using the true and estimated values of the aerodynamic parameters. A well matched frequency-response characteristics (Fig. 13) and close agreement between the estimated and true parameters (Table 4) justify the use of SIMDATA2 and ALGOPE1 for estimating the steady-state values of the aerodynamic parameters.

5.2 Parameter estimation using SIMDATA2

After establishing the fact that the indicial lift function has very little or negligible effect on the estimated parameters, the indicial lift effects were neglected for the further study of parameter estimation. Now, SIMDATA2 (included unsteadiness only in downwash), based on Equation (19) and Equation (21), was used to carry out the parameter estimation using ALGOPE1 ($\tilde{D} \neq 0$) and ALGOPE2 ($\tilde{D} = 0$). The coefficients F, G and H estimated earlier were used in the estimation algorithm ALGOPE1· The ML method was used to minimise the cost function (J) for the estimation of parameter vector (ξ) given by Equations (23) and (26) using ALGOPE1 and ALGOPE2, respectively.

$$\xi = [C_{L\alpha} \;\; C_{Lq} \; C_{L\delta e} \; C'_{m\alpha} \; C'_{mq} \; C'_{m\delta e}]^T \qquad \ldots (26)$$

When ALGOPE2 ($\tilde{D} = 0$) was used for parameter estimation using SIMDATA2, it was observed that the unsteady aerodynamic effects were absorbed in the estimated parameters. In particular, the following approximated parameters would be extracted instead of steady-state derivatives (parameters).

$$C'_{m\alpha} = (C_{m\alpha})_{ss} - \rho S_w \bar{c}_w \; C_{m\dot{\alpha}} \; C_{L\alpha}/4m \qquad \ldots (27(a))$$

$$C'_{mq} = (C_{mq})_{ss} + C_{m\dot{\alpha}} \qquad \ldots (27(b))$$

$$C'_{m\delta e} = (C_{m\delta e})_{ss} - \rho S_w \bar{c}_w \; C_{m\dot{\alpha}} \; C_{L\delta e}/4m \qquad \ldots (27(c))$$

Where

$$C_{m\alpha} = -2(l/\bar{c}_w)^2 \; (C_{L\alpha})_{t,ss} \; (\partial\varepsilon/\partial\alpha)_{l,ss} \qquad \ldots (27(d))$$

Table 5 presents the parameters estimated along with the Cramer-Rao bounds from SIMDATA2 ($\tilde{D} \neq 0$) using ALGOPE1 ($\tilde{D} \neq 0$) and ALGOPE2 ($\tilde{D} = 0$). It can be observed (Table 5) that the parameter $C_{m\dot{\alpha}}$ gets included in the parameter C'_{mq} and the value is very close to the difference between the parameters C_{mq} and C'_{mq}. Similar trend was observed in the case of other parameters such as $C'_{m\alpha}$ and $C'_{m\delta e}$.

Figure 14 compares the frequency-response characteristics of the angle-of-attack $\tilde{\alpha}/\tilde{\delta}_e$, pitch rate $\tilde{q}/\tilde{\delta}_e$ and vertical acceleration $\tilde{a}_z/\tilde{\delta}_e$ for a unit step elevator control input in terms of magnitude and phase generated by using the values of parameters estimated by ALGOPE1 ($\tilde{D} \neq 0$) and ALGOPE2 ($\tilde{D} = 0$). ($\tilde{\alpha}/\tilde{\delta}_e$, $\tilde{q}/\tilde{\delta}_e$ and $\tilde{a}_z/\tilde{\delta}_e$).

5.3 Parameter estimation from real flight data

Now, the compatible real flight data generated earlier (RSP1, RSP2, RSP3, RSP4 and EP1) for the semi-sweptback wing configuration

https://doi.org/10.1017/S0001924000006217 Published online by Cambridge University Press

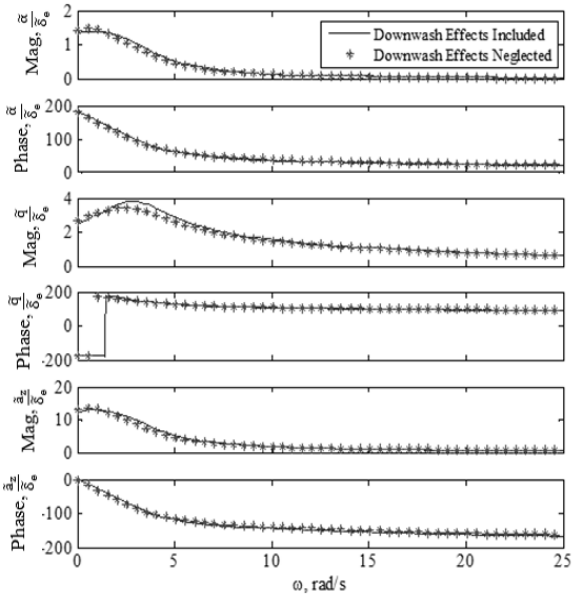


Figure 14. Comparison of magnitude and phase response ($\tilde{\alpha}/\tilde{\delta}_e$), ($\tilde{q}/\tilde{\delta}_e$) and ($\tilde{a}_z/\tilde{\delta}_e$).

Table 5
Parameter estimation using SIMDATA2

Parameters [True value]	Parameter estimation algorithm (model)	
	ALGOPE1 ($\tilde{D} \neq 0$)	ALGOPE2 ($\tilde{D} = 0$)
$C_{L\alpha}$ [5·0]	5·0 (0·0)	4·84 (0·0)
C_{Lq} [7·0]	7·0 (0·0)	10·2 (0·0)
$C_{L\delta e}$ [0·3]	0·3 (0·0)	0·32 (0·0)
$C_{m\alpha}$ [–0·4]	–0·4 (0·0)	-
C_{mq} [–8·0]	–8·0 (0·0)	-
$C_{m\delta e}$ [–0·8]	–0·8 (0·0)	-
$C'_{m\alpha}$	–	–0·29 (0·0)
C'_{mq}	–	–10·5 (0·0)
$C'm\delta e$	–	–0·8 (0·0)

( ) Cramer-Rao bounds

Table 6
Parameter estimation from real flight data using PEALGO1 ($\tilde{I} = 0$, $\tilde{D} \neq 0$)

Parameters	RSP1	RSP2	RSP3	RSP4	EP1
$C_{L\alpha}$	5·47(1·44)	5·83(1·00)	4·83(1·02)	5·24(0·78)	5·23(1·84)
C_{Lq}	4·93(5·97)	1·18(4·12)	74·9(20·9)	–1·19(4·37)	7·62(7·09)
$C_{L\delta e}$	0·48(0·11)	0·06 (0·08)	0·81 (0·10)	0·13 (0·06)	0·73 (0·15)
$C_{m\alpha}$	–0·37(0·03)	–0·43 (0·02)	–0·28 (0·07)	–0·49 (0·01)	–0·43 (0·01)
C_{mq}	–11·4(2·64)	–12·3 (1·70)	–5·05 (2·17)	–9·29 (1·35)	–7·72 (2·80)
$C_{m\delta e}$	–0·78(0·21)	–0·82 (0·14)	–0·50 (0·15)	–0·73 (0·11)	–0·71(0·25)

( ) Cramer-Rao bounds

of the Hansa-3 aircraft was used to estimate the parameter vector (ξ) given in Equation (23) and Equation (26) using ALGOPE1 ($\tilde{D} \neq 0$) and ALGOPE2 ($\tilde{D} = 0$), respectively. The ML method was applied to estimate ξ by minimising the cost function J.

Tables 6 and 7 present the parameters along with the Cramer-Rao bounds estimated from the real flight data sets using ALGOPE1 and ALGOPE2, respectively.

Table 6 presents the steady state parameters estimated by ALGOPE1· In this case also, it was observed that the parameters (Table 7), when estimated by ALGOPE2, included the unsteady aerodynamic effects as in the simulated case. However, the weak parameters such as C_{Lq} and $C_{L\delta e}$ could not be estimated correctly, but all the other parameters were estimated with a reasonable accuracy.

Table 7
Parameter estimation from real flight data using PEALGO2 ($\tilde{I} = 0$, $\tilde{D} = 0$)

Parameters	RSP1	RSP2	RSP3	RSP4	EP1
$C_{L\alpha}$	5·29(1·33)	5·65(0·95)	4·32(1·17)	5·17(0·77)	5·14(1·81)
C_{Lq}	6·01(5·67)	3·31(3·94)	60·6(15·6)	0·66(4·27)	7·41(6·78)
$C_{L\delta e}$	0·48(0·11)	0·03(0·07)	0·77(0·09)	0·12(0·06)	0·73(0·15)
$C'm\alpha$	–0·31(0·03)	–0·37(0·02)	–0·21(0·01)	–0·43(0·01)	–0·36(0·02)
$C'mq$	–13·1(2·12)	–13·9(1·54)	Í7·50(1·80)	–10·66(1·22)	–9·81(2·68)
$C'm\delta e$	–0·77(0·20)	–0·82(0·14)	–0·58(0·15)	–0·72(0·10)	–0·70(0·25)

( ) Cramer-Rao bounds

The graphical presentation of the measured and the estimated frequency response characteristics of the angle-of-attack ($\tilde{\alpha}$), pitch rate ($\tilde{q}$) and vertical acceleration ($\tilde{a}_z$) obtained during the parameter estimation has been shown only for one real flight data set i.e. RSP1· Similar behaviour of the frequency response characteristics was obtained (not shown) for other real flight data sets (RSP2, RSP3, RSP4 and EP1). Figures 15, 16 and 17 present the measured and computed frequency-response characteristics of $\tilde{\alpha}$, $\tilde{q}$ and $\tilde{a}_z$ in terms of real part, magnitude and phase, respectively during parameter estimation from real flight data using ALGOPE1·

Table 8
Effect of neglecting downwash effects completely from Estimation Algorithm

Difference	$C'_{m\alpha} - C_{m\alpha}$		$C'_{mq} - C_{mq}$		$C'_{m\delta e} - C_{m\delta e}$	
Flight	Estimated	Theoretical	Estimated	Theoretical	Estimated	Theoretical
SIMDATA2	0·11	0·06	–2·50	–2·41	0·000	0·003
RSP1	0·060	0·068	–1·820	–2·410	0·010	0·006
RSP2	0·060	0·073	–1·600	–2·410	0·000	0·000
RSP3	0·070	0·060	–2·450	–2·410	–0·080	0·010
RSP4	0·060	0·065	–1·370	–2·410	–0·010	0·001
EP1	0·067	0·065	–2·160	–2·410	0·010	0·009

Similarly, the measured and computed frequency-response characteristics of $\tilde{\alpha}$, $\tilde{q}$ and $\tilde{a}_z$ in terms of real part, magnitude and phase, respectively are presented in Figs 18, 19 and 20 when the use of ALGOPE2 was made for parameter estimation.

A well matched measured and estimated frequency response characteristics [Figs 15-20] confirm the high level of accuracy of the estimates for both the cases.

The effect of neglecting downwash effects completely from estimation algorithm was, further, analysed. The difference between the parameters [$C'_{m\alpha} - C_{m\alpha}$), ($C'_{mq} - C_{mq}$) and ($C'_{m\delta e}$) – $C_{m\delta e}$)] estimated by PEALGO1 and PEALGO2 was calculated and compared with the theoretical value calculated by using characteristics of the Hansa-3 aircraft (Table 1) and Equation (27). Table 8 presents the theoretical and estimated difference between the parameters for the simulated (SIMDATA2) as well as real flight data (RSP1, RSP2, RSP3, RSP4 and EP1). It can be observed (Table 8) that the values of theoretical and estimated difference between the parameters compare well for most of the cases. The low or negligible difference between the estimated and the theoretical values validates the estimation.

https://doi.org/10.1017/S0001924000006217 Published online by Cambridge University Press

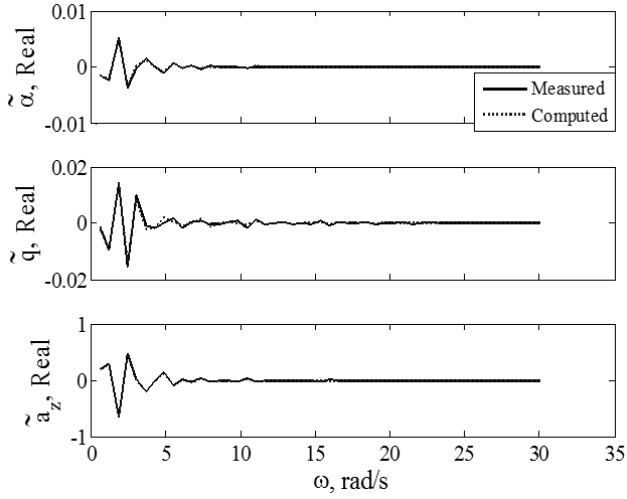


Figure 15. Measured and computed real response of $\tilde{\alpha}$, $\tilde{q}$ and $\tilde{\alpha}_z$ ($D \neq 0$); RSP1.

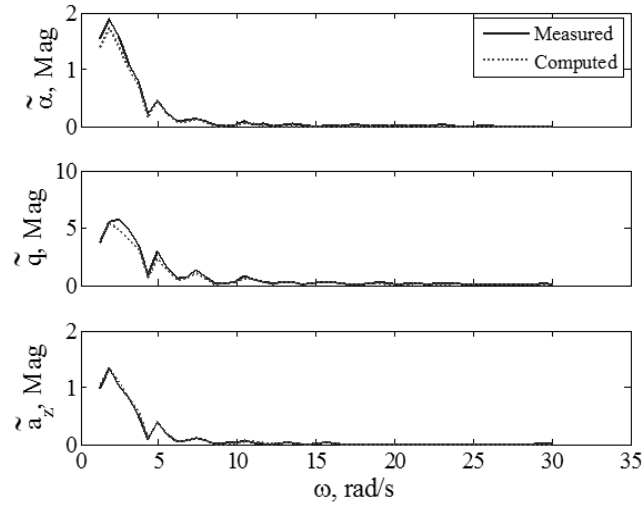


Figure 16. Measured and computed magnitude response of $\tilde{\alpha}$, $\tilde{q}$ and $\tilde{\alpha}_z$ ($D \neq 0$); RSP1.

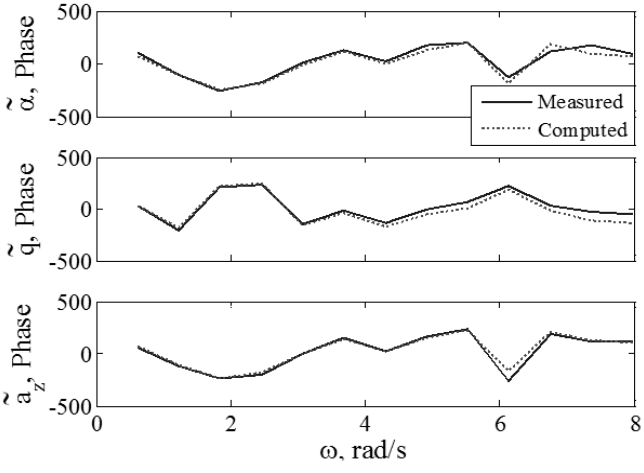


Figure 17. Measured and computed phase response of $\tilde{\alpha}$, $\tilde{q}$ and $\tilde{\alpha}_z$ ($D \neq 0$); RSP1.

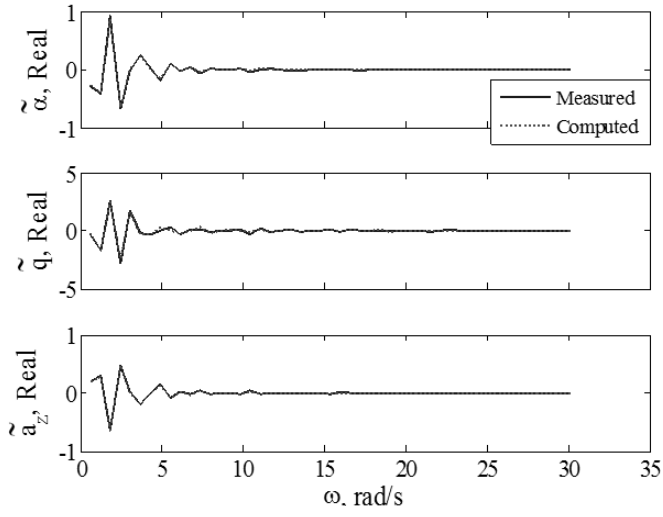


Figure 18. Measured and computed real response of $\tilde{\alpha}$, $\tilde{q}$ and $\tilde{\alpha}_z$ ($D = 0$); RSP1.

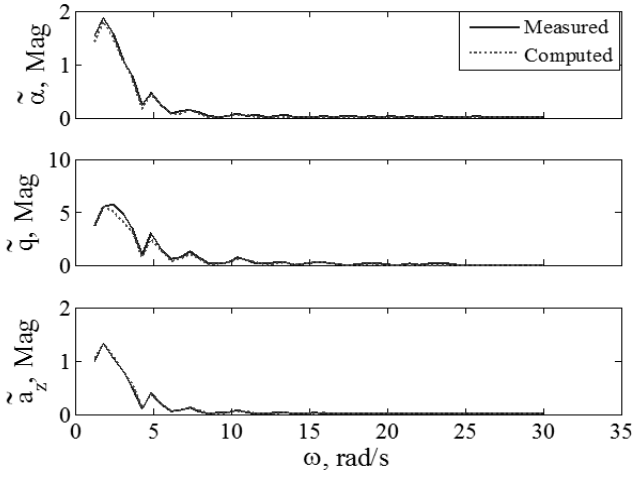


Figure 19. Measured and computed magnitude response of $\tilde{\alpha}$, $\tilde{q}$ and $\tilde{\alpha}_z$ ($D = 0$); RSP1.

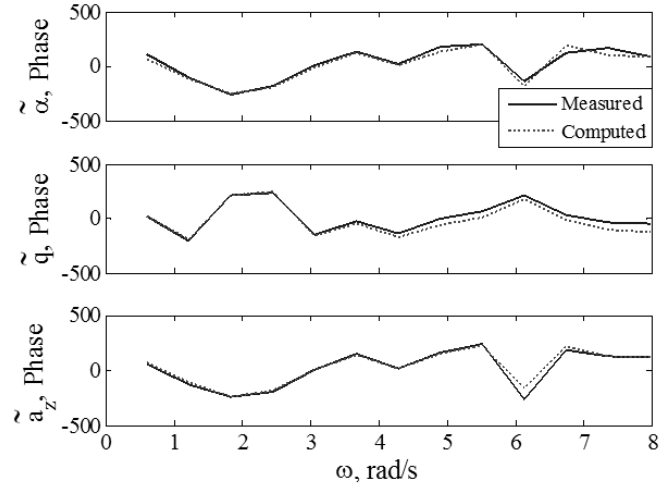


Figure 20. Measured and computed phase response of $\tilde{\alpha}$, $\tilde{q}$ and $\tilde{\alpha}_z$ ($D = 0$); RSP1.

https://doi.org/10.1017/S0001924000006217 Published online by Cambridge University Press

6.0 CONCLUSION

A simple vortex system was used to model unsteady aerodynamic effects into the longitudinal equations of motion. The task of the parameter estimation pertaining to the simulated and the real flight data of the Hansa-3 aircraft with a semi-sweptback wing configuration has been carried out in the frequency domain.

First, it was established that the indicial lift function had a little or negligible effect on estimated parameters. Subsequent calculations showed that the unsteady aerodynamic effects were adequately accounted for when the unsteady effects were included only in downwash. A parameter-estimation algorithm based on this formulation estimated the aerodynamic derivatives associated with steady-state motion. If unsteady effects were omitted from the estimation algorithm, it was observed that the estimated parameters included the effects of unsteady aerodynamics, i.e some of the estimated parameters could be interpreted as combinations of steady-state and acceleration derivatives. Use of the two estimation-algorithms, one including and the other omitting unsteady aerodynamic effects, provided a means of estimating some acceleration derivatives. For future work, the downwash model can be used to estimate lateral parameters for the sweptback wing configuration.

REFERENCES

1. ROSKAM, J. Methods for estimating Stability and control Derivatives for Conventional Subsonic Airplanes, Roskam Aviation and Engineering Corporation, 1973.
2. HAMEL, P.G. Aircraft Parameter Identification Methods and their Applications Survey and Future Aspects, AGARD, 15-104, November 1979, Paper 1.
3. ILIFF, K.W. Parameter estimation for flight vehicle, *J Guidance, Control and Dynamics*, 1989, **12**, (5), pp 609-622.
4. KLEIN, V. Estimation of aircraft aerodynamic parameter from flight data, *Progress in Aerospace Sciences*, 1989, **26**, (1), pp 1-77.
5. HAMEL, P.G. and JATEGAONKAR, R.V., The Evolution of Flight Vehicle System Identification, AGARD, DLR Germany, 8-10 May 1995.
6. KLEIN, V. and MORELLI, E.A. Aircraft System Identification – Theory and Practice, AIAA Education Series, Reston, Virginia, USA, 2006.
7 JATEGAONKAR, R.V. Flight Vehicle System Identification – A Time Domain Methodology, *AIAA Progress in Aeronautics and Astronautics*, **216**, AIAA, Reston, VA, USA, August 2006.
8. QUEIZO, M.J., WELLS, W.R. and KESKAR, D.A. Approximate Indicial Lift Function for Tapered, Swept Wings in Incompressible Flow, NASA, TP-1241, 1978.
9. QUEIZO, M.J., WELLS, W.R. and KESKAR, D.A. Inclusion of Unsteady Aerodynamics in Longitudinal Parameter Estimation from Flight Data, NASA, TP-1536, 1979.
10. WELLS, W.R. and QUEIZO, M.J. Simplified Unsteady Aerodynamic Concepts with Application to Parameters Estimation, AIAA Paper 77-1124, August 1977.
11. WELLS, W.R. and QUEIZO, M.J. Simplified unsteady aerodynamic concepts with application to parameters estimation, *J Aircr*, **16**, February 1979.
12. QUEIZO, M.J., WELLS, W.R. and KESKAR, D.A. Influence of Unsteady Aerodynamics on Extracted Aircraft Parameters, AIAA Paper 78-1343, August 1978.
13. GHOSH, A.K. Parameter Estimation of an Augmented Airplane Including Unsteady Effects, M.Tech Thesis, IIT Kanpur, India, January 1989.
14. KESKAR, D. Maximum Likelihood Identification of Aircraft Parameters with Unsteady Aerodynamic Modelling, 17th Aerospace Sciences Meeting, NY, USA, 15-17 January, 1979.
15. WELLS, W.R., BANDA, S.S. and QUAM, D.L. A model for unsteady effects in Lateral Dynamics for use in Parameter Estimation, AIAA Paper 79-1638, 1979.
16. WELLS, W.R. and QUAM, D.L. Model for unsteadiness in lateral dynamics for use in parameter estimation, *J Aircr*, 1979, **17**, (9).
17. SINGH, J. Unsteady Aerodynamic Modelling for Parameter Estimation from Flight Data, PhD Thesis, IIT Kanpur, India, April 1993.

Lecturer/Senior Lecturer in Aerospace Engineering

£29,972- £45,336 **Ref: 1187528**

We seek to appoint a Lecturer/Senior Lecturer to contribute to and enhance teaching and research/knowledge exchange in aerospace engineering within the Department of Engineering Design and Mathematics. Bristol and the West of England is a globally recognised hub for Aerospace, with a wide range of Aerospace organisations based locally. We are looking for an individual who can play a leading role in promoting links between the department and industry. You would be part of a team delivering high quality teaching and research/knowledge exchange in aerospace engineering and related disciplines, across all levels from UG level 1 to MSc. We would also welcome the post holder contributing to our Continuing Professional Development in Aerospace (CPDA) programme.

The principal role for the post holder will be to contribute to the Department's teaching in the area of aerospace engineering as well as supporting other areas of engineering as appropriate. Undergraduate subjects to be taught include Flight Mechanics, Aerodynamics and Aero-propulsion. It would be an advantage for the post holder to be able to teach aero-elasticity or aero-acoustics at Masters level. Experience of collaboration with industry is essential. There are opportunities to develop research and/or knowledge exchange.

Main duties and responsibilities

- Teaching and assessment of undergraduate, postgraduate and short course students and development of teaching materials for use in modules;
- Provision of support and guidance to students, covering both academic matters and other areas relevant to their performance as students;
- The recruitment, selection and admission of students, including activities to market the Department to prospective students;
- Development and management of modules;
- Scholarly and professional activity, which may include consultancy work, involvement in the activities of relevant professional institutions;
- Research, including the generation of research funding bids, conduct of research projects, publication of results and supervision of postgraduate research students;
- Participation and/or leadership of appropriate knowledge exchange and industrial/business collaboration activities with partners outside the university;
- Any other activity as determined by the Head of Department or Dean as required.

Applications for this post must be submitted using our online eRecruitment system, which can be accessed via our vacancies website

www.uwe.ac.uk/jobs

Closing date: 30 September 2011.

UWE is an equal opportunities employer.

UWE BRISTOL University of the West of England

Stonewall DIVERSITY CHAMPION

bettertogether

https://doi.org/10.1017/S0001924000006217 Published online by Cambridge University Press